

See discussions, stats, and author profiles for this publication at: <https://www.researchgate.net/publication/259294400>

Electrochemical Adsorption Properties and Inhibition of Brass Corrosion in Natural Seawater by Thiadiazole Derivatives: Experimental and Theoretical Investigation

ARTICLE *in* INDUSTRIAL & ENGINEERING CHEMISTRY RESEARCH · JANUARY 2012

Impact Factor: 2.59

READS

44

1 AUTHOR:



Joseph Raj Xavier

National Institute for Materials Science

14 PUBLICATIONS 33 CITATIONS

SEE PROFILE

Electrochemical Adsorption Properties and Inhibition of Brass Corrosion in Natural Seawater by Thiadiazole Derivatives: Experimental and Theoretical Investigation

Joseph Raj Xavier, S. Nanjundan, and Nallaiyan Rajendran*

Department of Chemistry, Anna University, Chennai 600 025, India

ABSTRACT: The electrochemical behavior of brass in natural seawater in the absence and presence of thiadiazole derivatives, namely, 2-amino-5-(4-methoxyphenyl)-1,3,4-thiadiazole (AMOPTD), 2-amino-5-(4-methylphenyl)-1,3,4-thiadiazole (AMPTD), 2-amino-5-(4-pyridinyl)-1,3,4-thiadiazole (APTD), and 2-amino-5-(4-nitrophenyl)-1,3,4-thiadiazole (ANPTD), has been investigated by electrochemical techniques such as potentiodynamic polarization and electrochemical impedance spectroscopy (EIS). The optimum concentration of the studied inhibitors showing the highest inhibition efficiency was also evaluated at five different temperatures in the range between 303 and 343 K. The inhibition efficiency was found to increase with increase in concentration of the inhibitors but decrease with rise in temperature for all the studied inhibitors except ANPTD. Thermodynamic and kinetic parameters for the adsorption process were determined. Quantum chemical approach was further used to calculate some electronic properties of the molecule in order to confirm any correlation between the inhibitive effect and molecular structure of the studied inhibitors. Inductively coupled plasma atomic emission spectroscopy (ICP-AES) analysis confirms that dezincification was minimized to a greater extent in the presence of the investigated inhibitors. Scanning electron microscopy (SEM), energy dispersive X-ray analysis (EDS), and Fourier transform infrared spectroscopy (FT-IR) observations of the brass surface confirmed the existence of such an adsorbed film.

1. INTRODUCTION

Copper and its alloys are used in marine environments, heat exchanger tubes in absorption refrigeration systems, and water distribution systems due to their excellent electrical and thermal conductivity, good machineability, corrosion resistance, and low cost.^{1–3} They have become the material of choice in the deposition of highly conductive interconnects on an integrated circuit. Brass is widely used as tubing material for condensers in cooling water systems. The majority of the marine propellers are made from copper and its alloys. Although copper and its alloys are resistant toward the influence of atmosphere and many chemicals, they are susceptible to corrosion problems such as dezincification and pitting corrosion in aggressive media. They corrodes easily in chloride-containing aqueous solutions.

The corrosion resistance of copper and its alloys is due to the formation of a cuprous oxide layer, Cu₂O, when exposed to the atmosphere. The chloride ion promotes the dissolution of both copper and zinc as evidenced by the selective dissolution of brass at various potentials in an aggressive chloride medium.⁴

One of the most important methods in the corrosion protection of brass is the use of organic inhibitors. Many of the well-known inhibitors are organic compounds containing nitrogen, sulfur, and oxygen atoms.^{5–7} It has been observed that many of the organic inhibitors act by adsorption on the metal surface via negatively charged centers where the inhibitor property is believed to relate to the polar groups and/or π-electrons.⁸ This phenomenon is influenced by the nature and surface charge of the metal, the type of aggressive medium, and the chemical structure of the inhibitors. A partial transfer of electrons from the donor atoms directly to the metal surface atoms can be viewed as a coordinative type of bond. Thus, in the case of heterocycles

containing nitrogen atoms, donation from either the polar nitrogen or the π-electrons would be expected. The vacant d orbitals present in the copper atom form coordinative bonds with atoms that are able to donate electrons. Interaction of the vacant d orbitals with the π-electrons of the rings containing conjugated bonds is also expected. Based on these results, more and more compounds containing numerous heteroatoms and functional groups are being developed and synthesized since it is noticed that they are responsible for good properties regarding corrosion inhibition because they enable chemisorption. The influence of various thiadiazole compounds on corrosion of copper in chloride media was studied.^{9–11} The inhibitor molecules are strongly adsorbed on copper, forming complexes with copper ions, and they prevent the formation of copper chloride and oxychloride complexes. Triazole compounds have been used as inhibitors to reduce the corrosion of brass in different media.^{12–14} The kinetics of the dissolution and dezincification mechanism of brass in chloride-containing systems has been investigated using electrochemical studies.^{15–17}

The aim of the present work is to investigate the electrochemical behavior of brass in natural seawater by electrochemical techniques such as potentiodynamic polarization and electrochemical impedance spectroscopy (EIS) in the presence and absence of thiadiazole derivatives, namely, 2-amino-5-(4-methoxyphenyl)-1,3,4-thiadiazole (AMOPTD), 2-amino-5-(4-methylphenyl)-1,3,4-thiadiazole (AMPTD), 2-amino-5-(4-pyridinyl)-1,3,4-thiadiazole (APTD), and 2-amino-5-(4-nitrophenyl)-1,3,4-thiadiazole (ANPTD),

Received: August 2, 2010

Accepted: November 12, 2011

Revised: November 12, 2011

Published: November 12, 2011

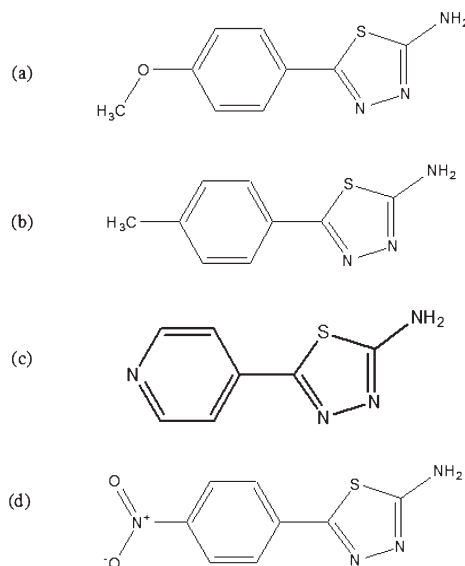


Figure 1. Chemical structures of investigated organic inhibitors: (a) 2-amino-5-(4-methoxyphenyl)-1,3,4-thiadiazole (AMOPTD), (b) 2-amino-5-(4-methylphenyl)-1,3,4-thiadiazole (AMPTD), (c) 2-amino-5-(4-pyridinyl)-1,3,4-thiadiazole (APTD), and (d) 2-amino-5-(4-nitrophenyl)-1,3,4-thiadiazole (ANPTD).

and 2-amino-5-(4-nitrophenyl)-1,3,4-thiadiazole (ANPTD). It is aimed to study the thermodynamic and quantum chemical parameters. It is also aimed to predict the thermodynamic feasibility of the inhibitors via coverage of the brass surface by the adsorbed compounds and to study the adsorption mechanisms of the studied thiadiazole derivatives on brass. The mode of coordination of the ligand to the metal surface was confirmed by Fourier transform infrared spectroscopy (FT-IR). The concentrations of dissolved copper and zinc in the electrolyte were calculated using inductively coupled plasma atomic emission spectroscopy (ICP-AES). The surface morphological studies were carried out using scanning electron microscopy (SEM), and the composition of brass surface was analyzed using energy dispersive X-ray analysis (EDS).

2. EXPERIMENTAL SECTION

2.1. Materials. AMOPTD, AMPTD, APTD, and ANPTD (Sigma-Aldrich, 98%) and absolute ethanol (C_2H_5OH , Fischer, 99.9%) were used as received. The electrolyte used was the natural seawater collected in a sterilized brown flask from Eliot beach on the southern coast of Chennai, India (Indian Ocean) containing Cl^- (20 400 mg L $^{-1}$), Na^+ (11 820 mg L $^{-1}$), Mg^{2+} (1010 mg L $^{-1}$), Ca^{2+} (394 mg L $^{-1}$), SO_4^{2-} (1250 mg L $^{-1}$), and HCO_3^- (219 mg L $^{-1}$), whereas others species were at lower concentrations. The pH was 8.3. The working electrode used for the study was a brass specimen having dimensions $1 \times 2.5 \times 0.1$ cm 3 and having the chemical composition of 65.3% Cu, 34.44% Zn, 0.1385% Fe, and 0.0635% Sn expressed in weight percent. The brass specimens were polished mechanically with different grades of silicon carbide papers (400–1200) and were thoroughly washed with double distilled water; then they were degreased in acetone using an ultrasonic vibrator and again thoroughly washed with double distilled water and dried. The concentration range of the inhibitors used for the study was

10^{-5} – 10^{-2} M. The structures of thiadiazole derivatives are shown in Figure 1.

2.2. Potentiodynamic Polarization Studies. An electrochemical cell with a three-electrode configuration was used to study the electrochemical measurements. Brass coupons with an exposed area of 0.28 cm^2 , a platinum foil of 1 cm^2 area, and silver/silver chloride (Ag/AgCl) in saturated KCl (Advance-Tech Controls Pvt. Ltd., India) were used as the working electrode, counter electrode, and reference electrode, respectively. The polarization experiments were carried out using a potentiostat/galvanostat (Model PGSTAT 12, AUTOLAB, The Netherlands) controlled by a personal computer with dedicated software (GPES, version 4.9.005). The polarization experiments were carried out for brass specimen at a scan rate of 1 mV/s in the presence and absence of inhibitors in natural seawater. The working electrode was immersed in natural seawater in the presence and absence of different concentrations of the inhibitors to which a current of -1.0 mA cm^{-2} was applied for 15 min to reduce oxides and then allowed to stabilize for 30 min. The cathodic and anodic polarization curves for brass specimen in the test solution were recorded from -600 to $+200$ mV. All the potentials reported here are with respect to the Ag/AgCl electrode.

2.3. Electrochemical Impedance Spectroscopy (EIS). Electrochemical impedance measurements were conducted using a potentiostat/galvanostat (Model PGSTAT 12, AUTOLAB, (ECO CHEMIE B.V. Netherlands, The Netherlands) with a frequency response analyzer (FRA). The impedance measurements were carried out at an open circuit potential after 30 min immersion of the brass electrode in the corrosive medium. The impedance data were acquired in the frequency range 100 kHz–50 mHz at 10 points per hertz decade with an ac voltage amplitude of ± 10 mV. The impedance spectra were fitted using a nonlinear least squares fitting procedure. The software EQUIVCRT modeled by B. A. Boukamp was used in this study for EIS data modeling.

2.4. Analysis of FT-IR Spectroscopy. The film formed on the brass surface in the presence of the inhibitor was washed with water, dried, and collected by scraping from the surface of the alloy for subsequent spectral analysis, namely FT-IR. FT-IR spectra of the inhibitors before and after adsorption on metal surface were recorded between 4000 and 400 cm^{-1} using 12 scans with a resolution of 1 cm^{-1} using a Perkin-Elmer Model 577 spectrometer.

2.5. Inductively Coupled Plasma Atomic Emission Spectroscopy (ICP-AES). The concentrations of Cu^{2+} and Zn^{2+} in the electrolytes, after the polarization experiments in the presence and absence of 10^{-2} M thiadiazole derivatives, were determined by ICP-AES. ICP-AES (ARCOS from M/s. Spectro, Germany) was used to measure the amount of dissolution of zinc and copper from the brass surface. The dezincification factor (z) was calculated using the equation¹⁸

$$z = \frac{[C_{Zn}/C_{Cu}]_{soln}}{[C_{Zn}/C_{Cu}]_{alloy}} \quad (1)$$

where $[C_{Zn}/C_{Cu}]_{soln}$ and $[C_{Zn}/C_{Cu}]_{alloy}$ are the ratios between the concentrations of zinc and copper in the solution and in the alloy, respectively.

2.6. SEM and EDS Investigations. A Philips Model XL30SFEG scanning electron microscope with an energy dispersive X-ray analyzer attached was used for surface analysis. The brass surface was prepared by keeping the electrodes for 1 h in electrolytes in the presence and absence of optimum concentrations of thiadiazole

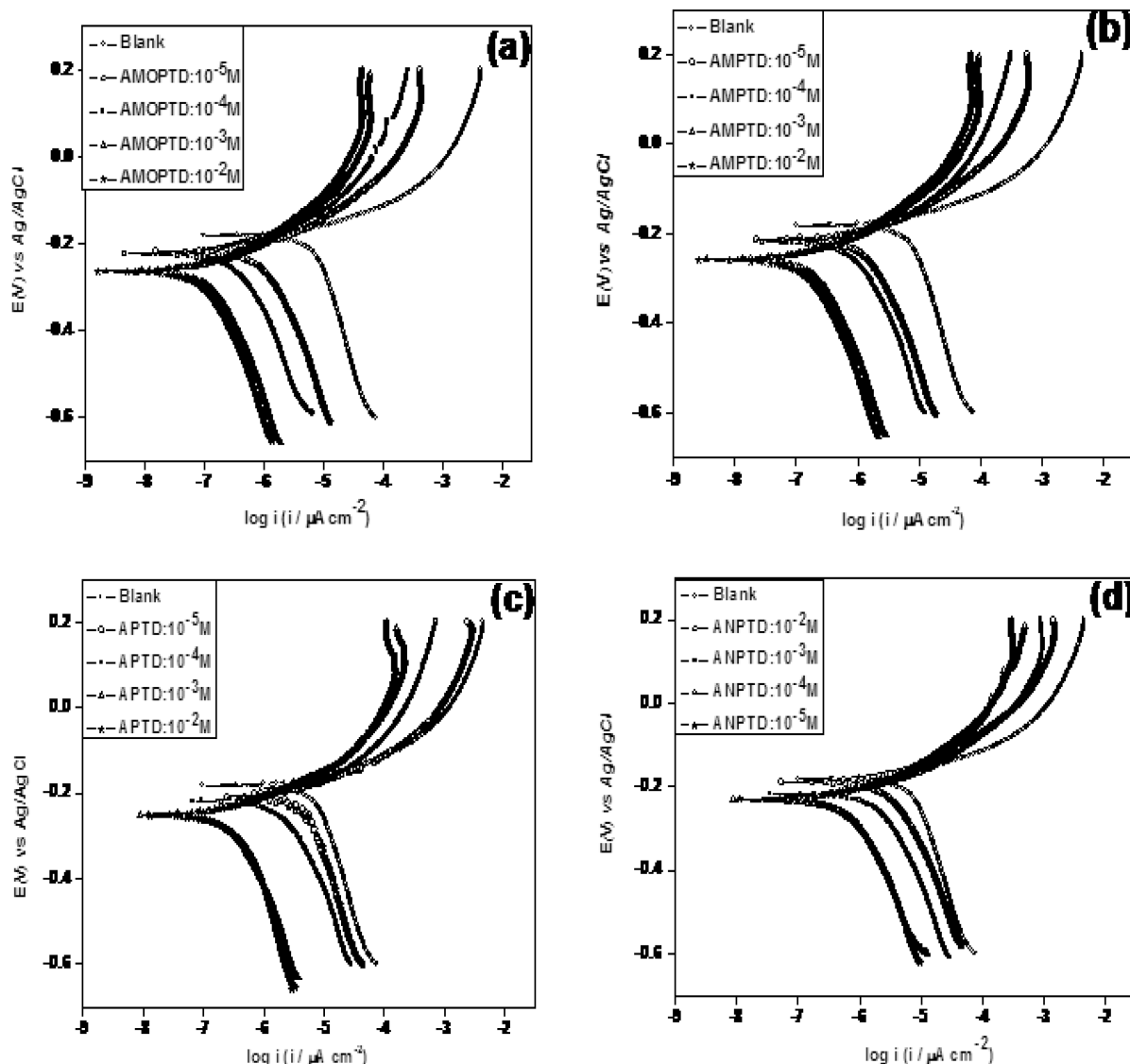


Figure 2. Potentiodynamic polarization curves for brass in natural seawater in the absence and presence of various concentrations of (a) AMOPTD, (b) AMPTD, (c) APTD, and (d) ANPTD.

derivatives. The brass specimens were then washed with distilled water, carefully dried, and analyzed using SEM/EDS.

3. RESULTS AND DISCUSSION

3.1. Potentiodynamic Polarization Studies. Potentiodynamic polarization experiments for brass in natural seawater in the presence and absence of AMOPTD, AMPTD, APTD, and ANPTD were carried out respectively and are shown in Figure 2. The corrosion current density (I_{corr}), corrosion potential (E_{corr}), and anodic β_a and cathodic β_c slopes, corrosion rates, were obtained by extrapolating the cathodic and anodic regions of the Tafel plots and are presented in Table 1. It is known from Figure 2 that both the anodic and cathodic reactions of brass corrosion were suppressed in the presence of the studied inhibitors in natural seawater and the suppression effect increased with the increase in the concentrations of AMOPTD, AMPTD, and APTD. The optimum concentration used is 10^{-3} M for AMOPTD, AMPTD, and APTD. In contrast, the optimum

concentration used is 10^{-4} M for ANPTD due to the presence of the electron-withdrawing nitro group. The inhibition efficiency (IE) was calculated using the following equation.¹⁹

$$\text{IE (\%)} = \frac{I_{\text{corr}} - I_{\text{corr(inh)}}}{I_{\text{corr}}} \times 100 \quad (2)$$

where I_{corr} and $I_{\text{corr(inh)}}$ correspond to the current densities of the uninhibited and inhibited solutions, respectively. As can be seen from Table 1, the corrosion currents decreased and the corrosion potentials shifted in the cathodic direction as the concentrations of the thiadiazole derivatives were increased, except for ANPTD. The inhibitive action of ANPTD in the concentration range 10^{-5} – 10^{-4} M could be attributed to adsorption of the molecules in a planar position. At 10^{-3} M adsorption through the $-\text{NO}_2$ group with the molecule perpendicular to the surface could result in reduction of the $-\text{NO}_2$ group to $-\text{NH}_2$, thus shifting the potential in the anodic direction and increasing the corrosion current.²⁰ The shift of corrosion potentials in the cathodic direction and decrease of corrosion currents with the

Table 1. Tafel Polarization Parameters for the Corrosion of Brass in Natural Seawater in the Absence and Presence of Different Concentrations (10^{-5} – 10^{-2} M) of AMOPTD, AMPTD, APTD, and ANPTD

compound	concn (M)	E_{corr} (mV)	I_{corr} ($\mu\text{A cm}^{-2}$)	β_c (mV/dec)	β_a (mV/dec)	CR ($\text{mm} \cdot \text{year}^{-1}$) $\times 10^{-3}$	IE (%)
blank	—	−181	2.65	36	67	110	—
AMOPTD	10^{-5}	−213	1.58	55	104	66.5	40.4
	10^{-4}	−223	0.50	64	121	20.7	81.1
	10^{-3}	−263	0.09	90	135	3.3	96.6
	10^{-2}	−265	0.08	91	137	3.2	97.1
AMPTD	10^{-5}	−210	1.59	54	103	67.1	39.9
	10^{-4}	−218	0.52	62	119	21.5	80.4
	10^{-3}	−257	0.12	86	130	4.5	95.5
	10^{-2}	−258	0.11	87	131	4.4	96.1
APTD	10^{-5}	−208	1.62	53	102	68.4	38.7
	10^{-4}	−217	0.77	55	105	32.3	71.0
	10^{-3}	−251	0.15	85	128	6.6	94.3
	10^{-2}	−252	0.14	86	129	6.5	94.7
ANPTD	10^{-5}	−230	0.53	63	120	22.8	79.9
	10^{-4}	−229	0.54	62	118	22.9	79.2
	10^{-3}	−208	2.21	41	81	79.9	16.4
	10^{-2}	−188	2.50	38	74	92.4	5.6

increase of AMOPTD, AMPTD, and APTD can be explained by the adsorption of these compounds at cathodic sites on the brass electrode. The highest inhibiting effect is seen with AMOPTD. In all cases, corrosion inhibition is under mixed control. All the thiadiazole derivatives demonstrate almost the same trend of decreasing corrosion rate with increase in concentration. The order of their efficiency is AMOPTD > AMPTD > APTD ≫ ANPTD.

3.2. Effect of Temperature. Polarization curves for brass in natural seawater at different temperatures (303–343 K) in the absence and in the presence of 10^{-3} M AMOPTD, AMPTD, and APTD and 10^{-4} M ANPTD are given in parts a, b, c, d, and e, respectively, of Figure 3. The corrosion current density increases and the inhibition efficiency decreases with the increase of temperature both in the absence and in the presence of inhibitors; thus both corrosion current density and inhibition efficiency of the studied inhibitors are temperature dependent in natural seawater. The decrease in inhibition efficiency with increase in temperature is due to the desorption of the inhibitor from the brass surface.

The Arrhenius equation was used to calculate the activation energy of the corrosion process.

$$I_{\text{corr}} = k \exp(-E_a/RT) \quad (3)$$

where k is the preexponential factor and E_a is the activation energy of the corrosion process. Figure 4 presents the Arrhenius plots of the natural logarithm of corrosion current density, $\ln I_{\text{corr}}$ against $1/T$ in the absence and presence of thiadiazole derivatives in natural seawater. Activation energy was found to decrease from 31.9 to 20.8 $\text{kJ} \cdot \text{mol}^{-1}$, from 30.4 to 18.9 $\text{kJ} \cdot \text{mol}^{-1}$, from 29.3 to 18.3 $\text{kJ} \cdot \text{mol}^{-1}$, and from 28.1 to 16.0 $\text{kJ} \cdot \text{mol}^{-1}$ for AMOPTD, AMPTD, APTD, and ANPTD, respectively, as the temperature increased from 303 to 343 K. The decrease in activation energy can be attributed to an appreciable decrease in the adsorption of the inhibitor on the surface of brass with increasing temperature. The increase in solution temperature slightly shifts E_{corr} in the positive direction and enhances both cathodic and anodic current densities. The decrease in inhibition

efficiency with increasing temperature may be due to the increase in desorption of AMOPTD.

3.3. Electrochemical Impedance Spectroscopic (EIS) Studies. Nyquist plots of brass in natural seawater in the presence and absence of AMOPTD, AMPTD, APTD, and ANPTD are shown in Figure 5. The impedance spectra were measured at the corrosion potential for each inhibitor at different concentrations. The Nyquist plots are significantly changed on addition of inhibitors; the impedance of the inhibited system increased with inhibitor concentration except for ANPTD. The impedance diagram in the presence of studied inhibitors shows a capacitive behavior throughout the measured frequency range. The impedance spectra in the presence of inhibitors can be modeled by three capacitive loops, and in the absence of inhibitors it can be modeled by using two capacitive loops. The analysis of these spectra was performed using the equivalent circuits^{21,22} shown in Figure 6.

It is observed that an acceptable accuracy of the fitting was obtained, as evinced by the chi-squared value (χ^2), which is on the order of 10^{-4} for all the experimental data. The parameters obtained by fitting the equivalent circuit and the calculated inhibition efficiency are listed in Table 2. Estimates of the margins of error calculated for the parameters are also given. Low χ^2 values and percentage errors indicate excellent agreement between the experimental and theoretical values, by using the constant phase element (CPE) in the fitting procedure. The impedance response typically reflects a distribution of reactivity that is commonly represented in equivalent electrical circuits as a CPE. The impedance can be expressed in terms of a CPE as

$$Z(\omega) = R + \frac{1}{(j\omega)^n C} \quad 0 \leq n \leq 1 \quad (4)$$

where Z is the impedance, ω is the angular frequency, R is the resistance, C is the capacitance, and n is a factor that satisfies the condition $0 \leq n \leq 1$, which indicates how far (0), or how close (1), the interface is from being treated as an ideal capacitor. The parameters n and C are independent of frequency. When $n = 1$, C has units of a capacitance, i.e., F cm^{-2} , and represents the capacity

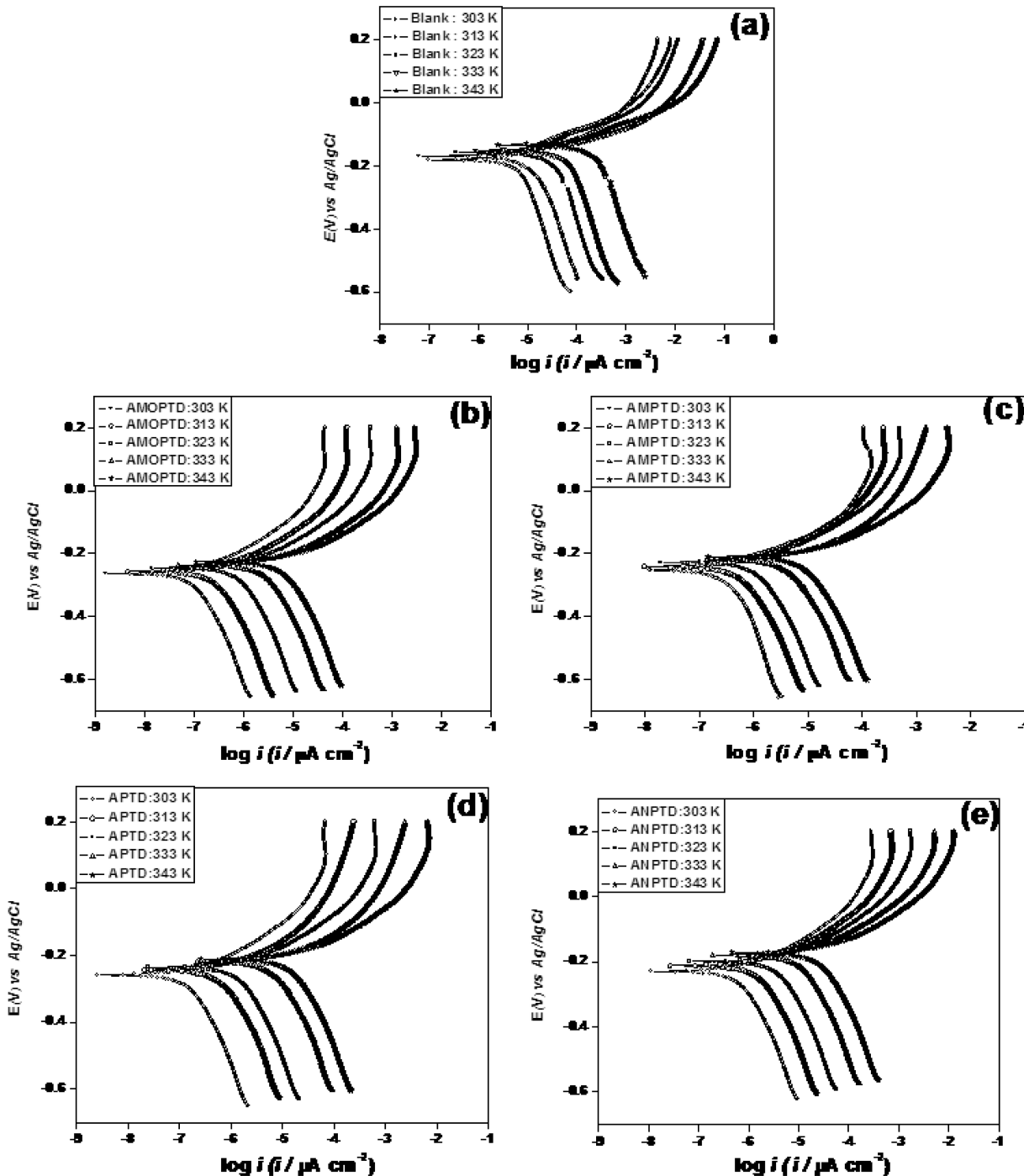


Figure 3. Effect of temperature on the potentiodynamic polarization curves for brass in natural seawater in the absence and presence of optimum concentrations of (a) blank (b) AMOPTD (10^{-3} M), (c) AMPTD (10^{-3} M), (d) APTD (10^{-3} M), and (e) ANPTD (10^{-4} M) in the range 303–343 K.

of the interface. Independent of the cause of CPE behavior, the phase angle associated with a CPE is independent of frequency.

The solution resistance (R_s) is very small. The most pronounced effect and highest charge transfer resistance is for AMOPTD, while ANPTD actually shows a decrease. R_{ct} values increase with concentration for all inhibitors studied except ANPTD. The value of the double-layer capacitance depends on many variables including electrode potential, temperature, ionic concentrations, types of ions, oxide layers, electrode roughness, impurity adsorption, etc. Table 2 indicates that, by increasing the

concentration of thiadiazole derivatives, C_{dl} values tend to decrease and the inhibition efficiency increases. The decrease in C_{dl} , which results from local dielectric constant decrease and/or an increase in the thickness of the electrical double layer, suggests that these molecules act by adsorption on the metal/solution interface.²³ It is clear that the highest values of R_{ct} are shown by AMOPTD followed by AMPTD and APTD, thus suggesting their enhanced inhibitor performance. In the presence of ANPTD, the R_{ct} decreased and the C_{dl} increased notably, approaching the values for the uninhibited solution. The reason for that might be

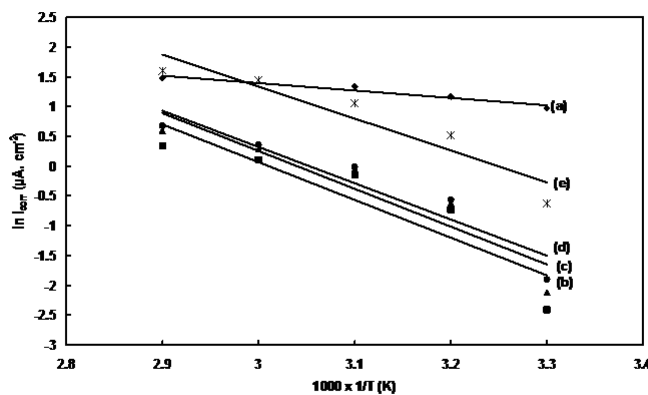


Figure 4. Arrhenius slopes calculated from corrosion current density for brass in natural seawater (a) blank and in the presence of (b) AMOPTD, (c) AMPTD, (d) APTD, and (e) ANPTD.

diffusion, along with desorption of ANPTD with partial adsorption of water or electrochemical reduction of the nitro group.²⁴

The Faradaic resistance that linked to the redox process involving corrosion products increases with increase in concentration of all the studied inhibitors except ANPTD, whereas the Faradaic capacitance decreases simultaneously with increase in concentration of all the studied inhibitors except ANPTD. From this it can be concluded that the corrosion products are less susceptible to the redox process with increase of concentration of the inhibitors except ANPTD and give better protection efficiency to the brass surface. The decrease in Faradaic resistance and increase in Faradaic capacitance with increase in concentration of ANPTD may be due to the presence of the electron-withdrawing nitro group leading to the desorption of ANPTD. It can be seen from Table 2 that R_f values increased and C_f values decreased for all inhibitors studied except ANPTD. This is attributed to the increase of true surface area which is partly due to the formation of the corrosion products and also to the roughening of electrode surface.

The percentage inhibition efficiency (IE) of thiadiazole derivatives on brass is calculated using the equation

$$\text{IE (\%)} = \frac{R_p(\text{inh}) - R_p}{R_p(\text{inh})} \times 100 \quad (5)$$

where $R_p(\text{inh})$ and R_p are polarization resistances in the presence and absence of inhibitors in electrolytes, respectively. The inhibition efficiency increases with increase in concentration, and a maximum inhibition efficiency of 97% was observed for 10^{-2} M AMOPTD. The maximum IE for 10^{-2} M AMPTD and 10^{-2} M APTD are 96 and 94%, respectively. The maximum inhibition efficiency for ANPTD at 10^{-5} M was found to be 80%, whereas at 10^{-2} M it was found to be 5%. The IE calculated from EIS shows the same trend as those estimated from polarization measurements; i.e., polarization measurements and EIS study complement each other well.

3.4. Adsorption Isotherm and Thermodynamic Parameters. The mode and extent of the interaction between an inhibitor and the brass surface can be studied by applying adsorption isotherms. The degree of surface coverage, θ , at different inhibitor concentrations of AMOPTD, AMPTD, APTD, and ANPTD in natural seawater was evaluated from electrochemical impedance spectroscopy measurements to explain the best isotherm to determine the adsorption process.

The linear relationship between θ values and C_{inh} is to be found in order to obtain the isotherm. Attempts were made to fit the θ values to various isotherms including Langmuir, Temkin, Frumkin, and Flory–Huggins. The best fit is obtained with the Langmuir isotherm. The Langmuir adsorption isotherm is given by²⁵

$$\frac{C_{\text{inh}}}{\theta} = C_{\text{inh}} + \frac{1}{K} \quad (6)$$

where C_{inh} is the concentration of inhibitor, θ is the fractional surface coverage, and K is the adsorption equilibrium constant. A plot of C_{inh}/θ against C_{inh} shows a straight line, indicating that adsorption follows the Langmuir adsorption isotherm as shown in Figure 7.

Thermodynamic parameters including the heat of adsorption, free energy of adsorption, and entropy of adsorption are important in the explanation of the corrosion inhibition mechanism. The free energy of adsorption (ΔG_{ads}) can be obtained from the equation²⁶

$$K_{\text{ads}} = \frac{1}{55.5} \exp\left(\frac{-\Delta G_{\text{ads}}}{RT}\right) \quad (7)$$

where ΔG_{ads} is the free energy of adsorption, R is the universal gas constant, T is the thermodynamic temperature, and 55.5 is the number of moles of water in solution expressed in mol L⁻¹. The heat of adsorption (ΔH_{ads}) can be calculated according to the van't Hoff equation:

$$\ln K_{\text{ads}} = \frac{-\Delta H_{\text{ads}}}{RT} + \text{constant} \quad (8)$$

where ΔH_{ads} and K_{ads} are the adsorption heat and adsorptive equilibrium constant, respectively.

To calculate the heat of adsorption, $\ln K_{\text{ads}}$ was plotted against $1/T$. The straight lines were obtained with slope equal to $-\Delta H_{\text{ads}}/RT$, and then the entropy of adsorption can be obtained at various temperatures using the equation

$$\Delta G_{\text{ads}} = \Delta H_{\text{ads}} - T\Delta S_{\text{ads}} \quad (9)$$

Figure 8 shows the relation between $\ln K_{\text{ads}}$ and $1/T$ for AMPTD, AMOPTD, ANPTD, and APTD, respectively, and the thermodynamic parameters obtained are given in Table 3. The values of ΔG_{ads} are negative, and they decrease as the inhibition efficiencies increase. This shows the spontaneity of the adsorption process and the stability of the adsorbed layer on the brass surface. It is known from Table 3 that the ΔG_{ads} values of -25 to -42 kJ/mol indicate the chemisorption mode. As the temperature increases, the value of the free energy of adsorption decreases negatively, indicating desorption of the studied inhibitors. In the present work, the calculated ΔG_{ads} values for 10^{-3} M concentration are -36.0 , -35.2 , -34.6 , and -36.7 kJ/mol for AMOPTD, AMPTD, APTD, and ANPTD (10^{-4} M) at 30 °C, respectively. These values are more negative than -20 kJ/mol, indicating the chemisorption of inhibitor molecules on the metal surface. It is observed from Table 3 a limited decrease in the absolute value of ΔG_{ads} with increase in temperature, indicating that adsorption is unfavorable with increasing temperature and that physisorption and chemisorption have equal contributions in the adsorption mechanism.

ΔH_{ads} is another criterion from which the mode of adsorption based on the absolute value can be probed. Generally, an endothermic process is explicit to chemisorption, while an

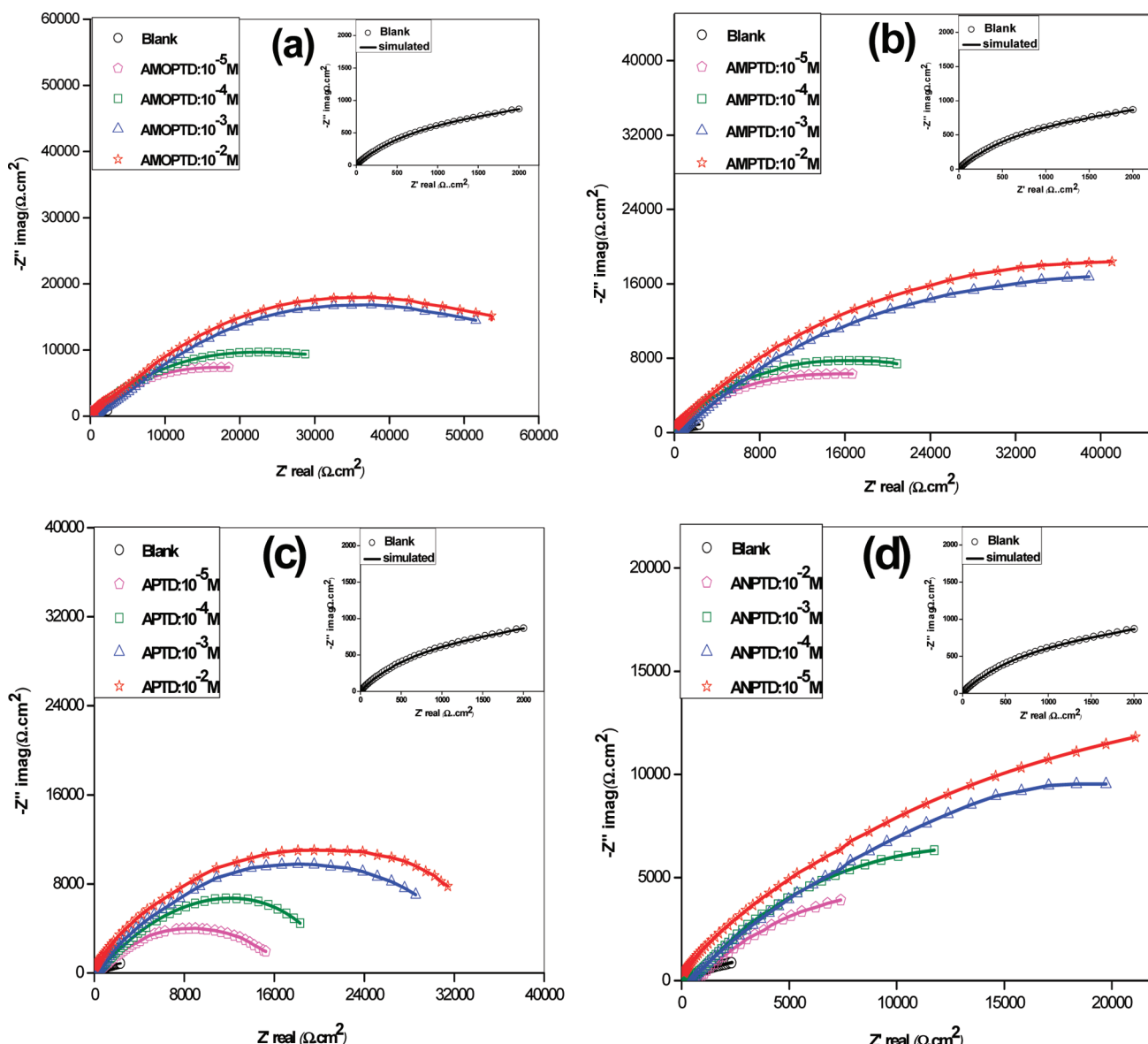


Figure 5. Nyquist plots of brass electrode in natural seawater in the absence and in the presence of different concentrations of thiadiazole derivatives: (a) AMOPTD, (b) AMPTD, (c) APTD, and (d) ANPTD. The lines correspond to the fitted data.

exothermic adsorption process designates either physisorption or chemisorption.²⁷ In an exothermic adsorption, the adsorption mode is judged based on the absolute value of ΔH_{ads} . An absolute value of enthalpy of adsorption lower than 40 kJ/mol indicates physical adsorption, and values approaching 100 kJ/mol indicate chemical adsorption. The ΔH_{ads} values of inhibitors at 10^{-3} M concentration of AMOPTD, AMPTD, APTD, and ANPTD (10^{-4} M) are -49.8 , -52.8 , -51.6 , and -360.5 kJ/mol at 30°C , respectively, indicating that the adsorption is an exothermic process.²⁸ In the present case, the absolute values of enthalpy of the studied inhibitors are higher than 40 kJ/mol, confirming chemisorption.

All values of ΔS_{ads} are negative in the adsorption process; inhibitor molecules are adsorbed in an orderly fashion onto the brass surface, causing a decrease in entropy.²⁹ The negative values of ΔS_{ads} are expected as the adsorption process is accompanied by a decrease in the disorder of the system due

to the adsorption of the free thiadiazole derivatives onto the brass surface. The decrease in K_{ads} with increasing temperature indicates a decrease in the extent of adsorption.³⁰ It is evident from Table 3 that K_{ads} decreased with increasing temperature. It is well-known that higher values of K_{ads} imply greater adsorption power of an inhibitor onto the brass surface. The value of the constant K_{ads} decreases with increasing temperature, indicating that the interactions between the adsorbed molecules and the metal surface are weakened and, consequently, the adsorbed molecules become easily removable.

3.5. Quantum Chemical Calculations. Some of the key quantum chemical parameters such as the energy of the highest occupied molecular orbital (E_{HOMO}), the energy of the lowest unoccupied molecular orbital (E_{LUMO}), and the dipole moment (μ) were computed using the PM3 method to investigate the effect of molecular structure on the inhibition mechanism and inhibition efficiency. E_{HOMO} is often associated with the capacity

of a molecule to donate electrons. Table 4 shows the energy (in electronvolts) of the highest occupied molecular orbital (HOMO) and the lowest unoccupied molecular orbital (LUMO) for inhibitors. It has been reported that the higher the HOMO energy (E_{HOMO}) level of the inhibitor, the greater is the ease of offering electrons to unoccupied d orbitals of copper and zinc and the greater the inhibition efficiency. The present

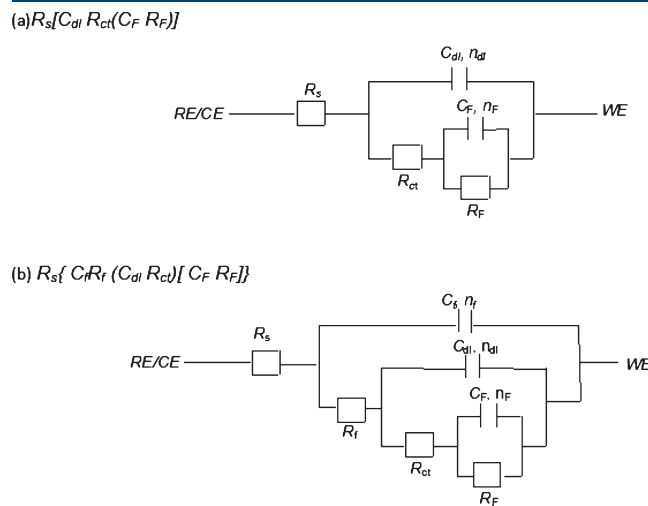


Figure 6. Equivalent electrical circuits used for computer fitting of the experimental data for the brass electrode in natural seawater (a) in the absence and (b) in the presence of AMOPTD, AMPTD, APTD, and ANPTD compounds: (a) $R_s[C_{dl}R_{ct}(C_F R_F)]$; (b) $R_s[C_F R_f(C_{dl} R_{ct})[C_F R_F]]$.

results show that E_{HOMO} and E_{LUMO} decrease in the order AMOPTD > AMPTD > APTD \gg ANPTD, which is parallel to the order of inhibition efficiency. The difference between HOMO and LUMO levels is defined as the energy gap (ΔE), which is equal to the energy needed to excite an electron from a highest occupied into a lowest unoccupied MO.³¹ Generally, the

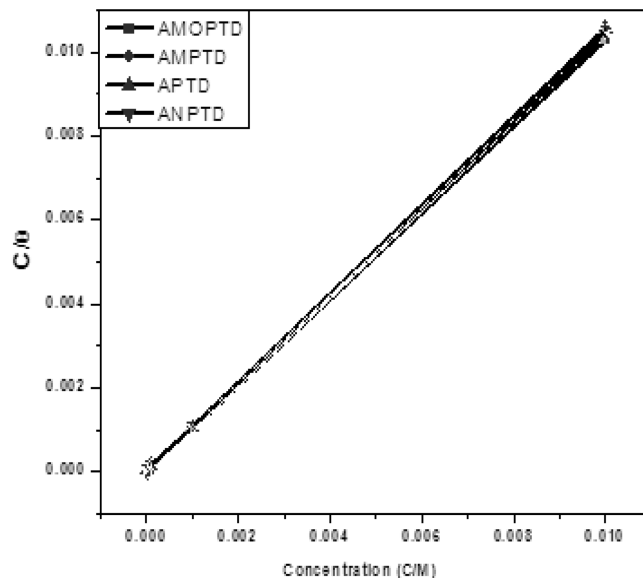


Figure 7. Langmuir adsorption isotherm of brass in natural seawater containing various concentrations (10^{-2} – 10^{-5} M) of AMOPTD, AMPTD, APTD, and ANPTD.

Table 2. Electrochemical Parameter Values for Brass Corrosion Calculated by Nonlinear Least Square Regression of the Impedance Data Using the Electrical Equivalent Circuits^a

inhibitor concn (M)	R_s ($\text{k}\Omega \text{ cm}^2$)	R_f ($\text{k}\Omega \text{ cm}^2$)	C_f ($\mu\text{F cm}^{-2}$)	n_f	R_{ct} ($\text{k}\Omega \text{ cm}^2$)	C_{dl} ($\mu\text{F cm}^{-2}$)	n_{dl}	R_F ($\text{k}\Omega \text{ cm}^2$)	C_F ($\mu\text{F cm}^{-2}$)	n_F	$\chi^2 \times 10^{-4}$	IE (%)
blank	46 ± 0.3	—	—	—	2.8 ± 0.2	155.1 ± 0.7	0.68	3.3 ± 0.3	25.4 ± 0.5	0.67	2.5	—
AMOPTD												
10^{-5}	0.2 ± 0.8	2.2 ± 0.2	7.3 ± 0.3	0.90	4.0 ± 0.1	8.2 ± 0.2	0.89	4.1 ± 0.5	6.5 ± 0.1	0.90	1.3	40.9
10^{-4}	0.3 ± 0.4	5.0 ± 0.5	4.3 ± 1.1	0.91	12.2 ± 0.5	6.1 ± 0.1	0.90	15.0 ± 1.1	4.2 ± 0.2	0.90	2.6	81.1
10^{-3}	0.5 ± 0.5	17.1 ± 1.1	1.5 ± 0.5	0.93	81.4 ± 0.3	2.3 ± 0.5	0.91	88.9 ± 0.1	1.3 ± 0.1	0.92	3.1	96.8
10^{-2}	0.5 ± 0.7	20.1 ± 0.9	1.4 ± 0.2	0.94	86.8 ± 0.2	2.1 ± 0.1	0.91	95.8 ± 0.4	1.3 ± 0.1	0.92	4.7	97.0
AMPTD												
10^{-5}	0.2 ± 1.1	2.1 ± 0.3	8.2 ± 1.6	0.90	3.9 ± 0.5	9.6 ± 0.9	0.88	4.1 ± 0.2	7.7 ± 0.6	0.88	1.2	39.9
10^{-4}	0.2 ± 0.4	4.7 ± 0.7	6.6 ± 0.4	0.90	12.1 ± 1.2	7.2 ± 0.6	0.89	14.3 ± 0.5	5.3 ± 0.1	0.90	1.6	80.5
10^{-3}	0.5 ± 1.2	13.8 ± 1.2	2.3 ± 0.1	0.92	56.5 ± 0.2	2.4 ± 0.2	0.90	69.7 ± 0.1	2.1 ± 0.5	0.92	2.9	95.7
10^{-2}	0.5 ± 1.3	14.9 ± 1.1	2.2 ± 1.2	0.93	59.9 ± 0.6	2.3 ± 1.2	0.91	73.0 ± 1.5	2.1 ± 0.1	0.92	3.1	95.9
APTD												
10^{-5}	0.2 ± 0.3	2.0 ± 1.5	13.4 ± 1.4	0.89	3.8 ± 1.1	14.7 ± 0.1	0.88	4.0 ± 1.3	12.0 ± 0.3	0.88	2.2	38.5
10^{-4}	0.2 ± 0.9	3.4 ± 0.6	10.8 ± 0.5	0.90	8.5 ± 0.8	11.8 ± 0.1	0.89	8.9 ± 0.4	9.1 ± 0.4	0.89	1.4	70.9
10^{-3}	0.4 ± 1.3	9.1 ± 1.1	7.1 ± 1.1	0.91	42.4 ± 1.1	7.6 ± 1.1	0.89	43.8 ± 0.9	5.9 ± 0.1	0.90	4.1	93.6
10^{-2}	0.4 ± 0.1	11.0 ± 0.2	6.9 ± 0.1	0.92	45.9 ± 0.3	7.4 ± 0.4	0.90	48.0 ± 0.1	5.5 ± 0.6	0.90	1.1	94.2
ANPTD												
10^{-5}	0.2 ± 1.2	4.7 ± 1.5	7.9 ± 0.2	0.88	12.1 ± 0.1	9.3 ± 0.2	0.87	13.3 ± 0.8	7.8 ± 0.9	0.88	1.9	79.9
10^{-4}	0.2 ± 0.2	4.0 ± 1.2	8.0 ± 0.9	0.87	12.0 ± 0.5	10.5 ± 1.1	0.86	13.3 ± 1.4	8.7 ± 0.6	0.86	1.5	79.3
10^{-3}	0.01 ± 0.7	0.4 ± 0.1	28.9 ± 1.3	0.62	1.9 ± 1.2	29.3 ± 0.6	0.61	4.9 ± 1.2	27.6 ± 1.2	0.61	2.7	16.4
10^{-2}	0.03 ± 1.4	0.4 ± 0.8	52.3 ± 1.1	0.52	1.2 ± 0.9	54.2 ± 0.1	0.51	4.9 ± 0.4	51.2 ± 1.9	0.52	3.3	5.3

^a $R_p(\text{inh}) = R_p + R_{ct} + R_F$ and $R_p = R_{ct} + R_F; R_s$, electrolyte resistance; R_{ct} , charge transfer resistance; C_{dl} , charge transfer capacitance; R_F , Faradaic resistance; C_F , Faradaic capacitance; R_f , film resistance; C_f , capacitance due to surface film; n_f , n_{dl} , and n_F , coefficients representing the depressed characteristic of the three capacitive loops.

correlation between ΔE values of 7.36, 7.42, 7.55, and 7.94 eV respectively, for AMOPTD, AMPTD, APTD, and ANPTD and their inhibitor efficiencies (Tables 1 and 2) show that higher efficiency can be related to a lower energy difference; i.e., molecules exhibiting lower energy difference readily undergo a charge transfer interaction with the metal surface. The low ΔE will yield good inhibition efficiencies, because the energy needed to remove an electron from the last occupied orbital will be low.³² Similarly low values of the dipole moment will favor the accumulation of inhibitor molecules on the metallic surface. The dipole moment is very high for ANPTD (10.26 D), and the negative charge density in the molecule is high on the two oxygen atoms. Poor inhibitive properties and near acceleration, as found for ANPTD, are a consequence of its specific electronic structure.

3.6. Inductively Coupled Plasma Atomic Emission Spectroscopic (ICP-AES) Analysis. The concentrations of copper and zinc in solutions containing 10^{-3} M thiadiazole derivatives after impedance and polarization measurements were determined

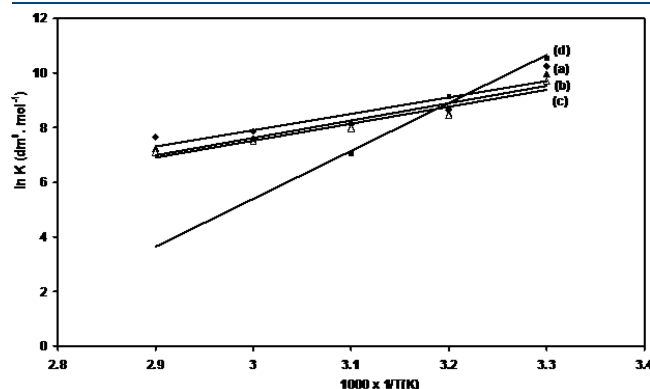


Figure 8. Adsorption isotherm plot for $\ln K$ versus $1/T$.

Table 3. Thermodynamic and Kinetic Parameters for the Adsorption of Studied Inhibitors in Natural Seawater on the Brass Surface at Different Temperatures (303–343 K)

compound	temperature (K)	K_{ads} ($\text{dm}^3 \cdot \text{mol}^{-1}$)	ΔG_{ads} ($\text{kJ} \cdot \text{mol}^{-1}$)	ΔH_{ads} ($\text{kJ} \cdot \text{mol}^{-1}$)	ΔS_{ads} ($\text{J} \cdot \text{mol}^{-1} \cdot \text{K}^{-1}$)	E_a ($\text{kJ} \cdot \text{mol}^{-1}$)
AMOPTD	303	28412	-36.0	-49.8	-45.7	31.90
	313	5729	-33.0	-49.8	-53.7	24.43
	323	3401	-32.6	-49.8	-53.2	22.21
	333	2580	-32.9	-49.8	-50.8	21.43
	343	2107	-33.3	-49.8	-48.2	20.84
AMPTD	303	21075	-35.2	-52.9	-58.4	30.42
	313	4981	-32.6	-52.9	-64.8	23.76
	323	3032	-32.3	-52.9	-63.7	21.90
	333	1970	-32.1	-52.9	-62.3	20.21
	343	1394	-32.1	-52.9	-60.6	18.92
APTD	303	16668	-34.6	-51.6	-55.9	29.27
	313	4666	-32.4	-51.6	-61.1	23.45
	323	2869	-32.2	-51.6	-60.0	21.41
	333	1785	-31.9	-51.6	-59.2	19.72
	343	1212	-31.7	-51.6	-57.8	18.30
ANPTD	303	38031	-36.7	-145.9	-360.5	28.12
	313	9227	-34.2	-145.9	-356.8	22.41
	323	1138	-29.7	-145.9	-338.8	16.04
	333	-	-	-	-	-
	343	-	-	-	-	-

from inductively coupled plasma atomic emission spectroscopic (ICP-AES) analysis. The dezincification (z) factors for brass in the absence and presence of 10^{-3} M AMOPTD, AMPTD, and APTD and 10^{-4} M ANPTD in natural seawater were calculated from the ICP-AES data, and the results are given in Table 5. The results show that both copper and zinc were present in the electrolyte in very small quantities and the copper to zinc ratio was found to be less than that of the bulk alloy. This is due to the surface barrier arising out of the growth of surface film of inhibitor on the metal surface as well as the corrosion products Cu_2O and ZnO . It is

Table 4. Quantum Chemical Parameters of AMOPTD, AMPTD, APTD, and ANPTD

compound	$-E_{\text{HOMO}}$ (eV)	$-E_{\text{LUMO}}$ (eV)	ΔE (eV)	μ (D)
AMOPTD	8.54	1.18	7.36	3.95
AMPTD	8.57	1.15	7.42	4.74
APTD	8.91	1.36	7.55	6.16
ANPTD	9.49	1.55	7.94	10.26

Table 5. Effect of AMOPTD, AMPTD, APTD, and APTD on the Dezincification of Brass in Natural Seawater at Optimum Concentration (10^{-3} M) for All Inhibitors Except ANPTD (10^{-4} M)

inhibitor	solution analysis (10^{-8} M)			inhibition (%)	
	Cu	Zn	dezincification factor (z)	Cu	Zn
blank	74	1725	43.29	—	—
AMOPTD	4	26	12.04	94.5	98.5
AMPTD	5	45	16.67	93.2	97.4
APTD	6	61	18.83	91.9	96.5
ANPTD	67	1525	42.15	9.5	11.6

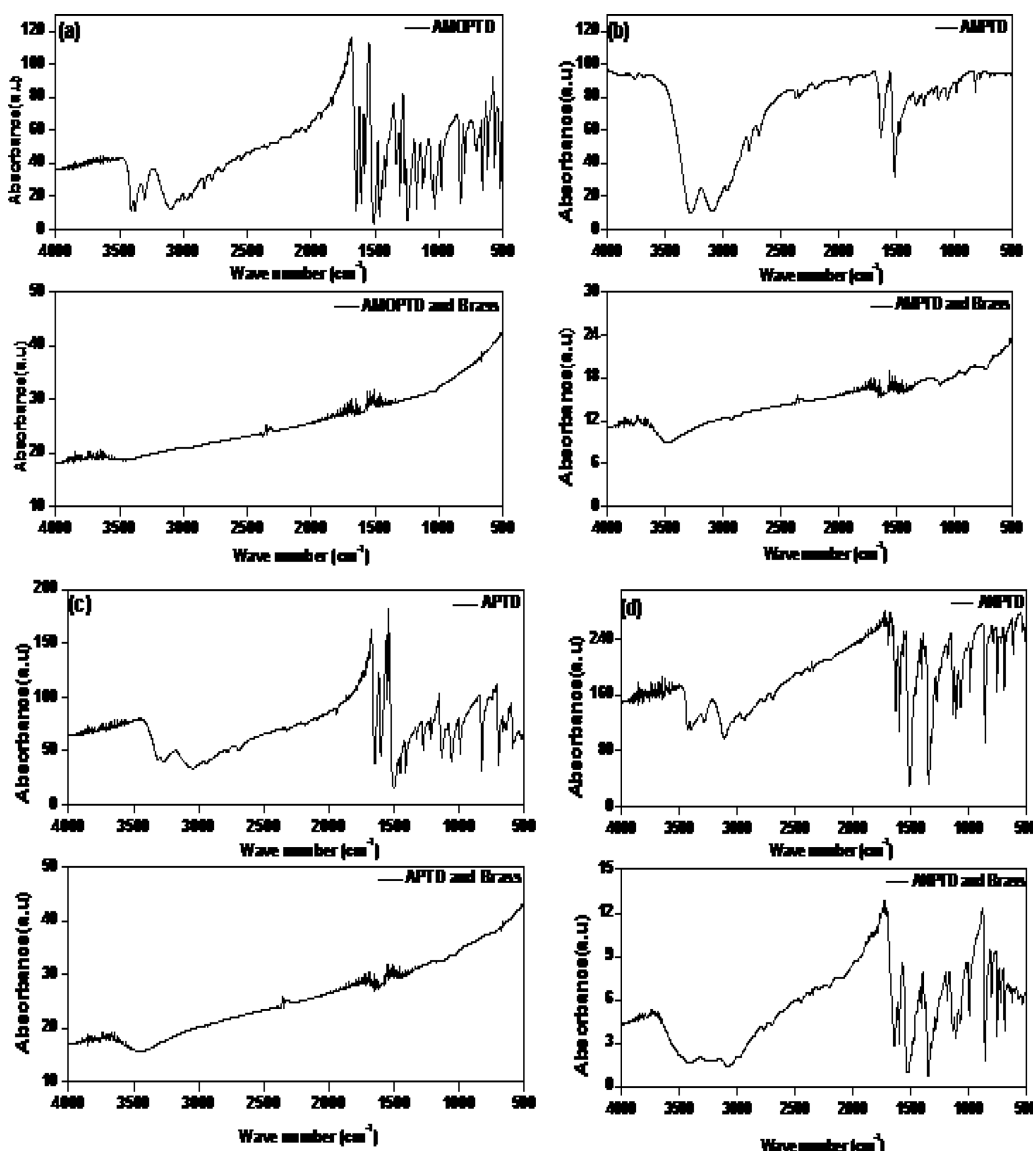


Figure 9. FT-IR spectra for AMOPTD, AMPTD, APTD, and ANPTD compounds and corresponding spectra after adsorption of the inhibitors on brass in (a)–(d).

known from Table 5 that dezincification was much higher in the absence of inhibitors, while dezincification was much lower in the presence of 10^{-3} M concentration of AMOPTD, AMPTD, and APTD. On the other hand, in the presence of ANPTD, the dezincification factor was predominant upon increasing the concentration. Much higher amounts of copper and zinc for ANPTD than for AMOPTD were found, suggesting the dissolution of copper and zinc (i.e., more rapid corrosion) in the presence of ANPTD. This indicates that AMOPTD, AMPTD, and APTD are able to minimize the dissolution of both zinc and copper. These values correlate with the corrosion rate and inhibition efficiency obtained by electrochemical methods (Tables 1 and 2).

3.7. FT-IR Spectroscopic Studies. The FT-IR spectra obtained for AMOPTD, AMPTD, APTD, and ANPTD and the corresponding spectra after adsorption of the inhibitors on brass are presented in Figure 9. The N–H stretching vibration due to the surface films of AMOPTD, AMPTD, APTD, and ANPTD compounds were observed at 3454, 3497, 3448, and 3401 cm^{-1} , respectively, indicating the complex formation with metal involving

the NH_2 group. The strong peaks at 1604, 1618, 1603, and 1599 cm^{-1} are attributed to the (NH) in-plane bending vibrations of the surface films of the AMOPTD, AMPTD, APTD, and ANPTD compounds, respectively. The bands at 1412, 1492, 1439, and 1407 cm^{-1} are assigned to the stretching vibrations of the C=N group in the ring for the surface films of AMOPTD, AMPTD, APTD, and ANPTD compounds, respectively. This indicates that there is a coordination of the ring to the metal surface. The ring N–N stretching vibrations for the compounds AMOPTD, AMPTD, APTD, and ANPTD are observed respectively at 1012, 1020, 1011, and 1071 cm^{-1} . The strong bands at 1579, 1472, 1552, and 1596 cm^{-1} are due to the C=C stretching vibration of AMOPTD, AMPTD, APTD, and ANPTD, respectively. The ring C–S vibration for the compounds AMOPTD, AMPTD, APTD, and ANPTD are observed respectively at 658, 691, 698, and 690 cm^{-1} .

The strong peak at 1266 cm^{-1} for AMOPTD is due to the aryl–O group. The strong peaks at 1173 and 1031 cm^{-1} for AMOPTD are attributed to the alkyl–O group. The symmetrical and asymmetrical C–H stretching vibrations due to the CH_3

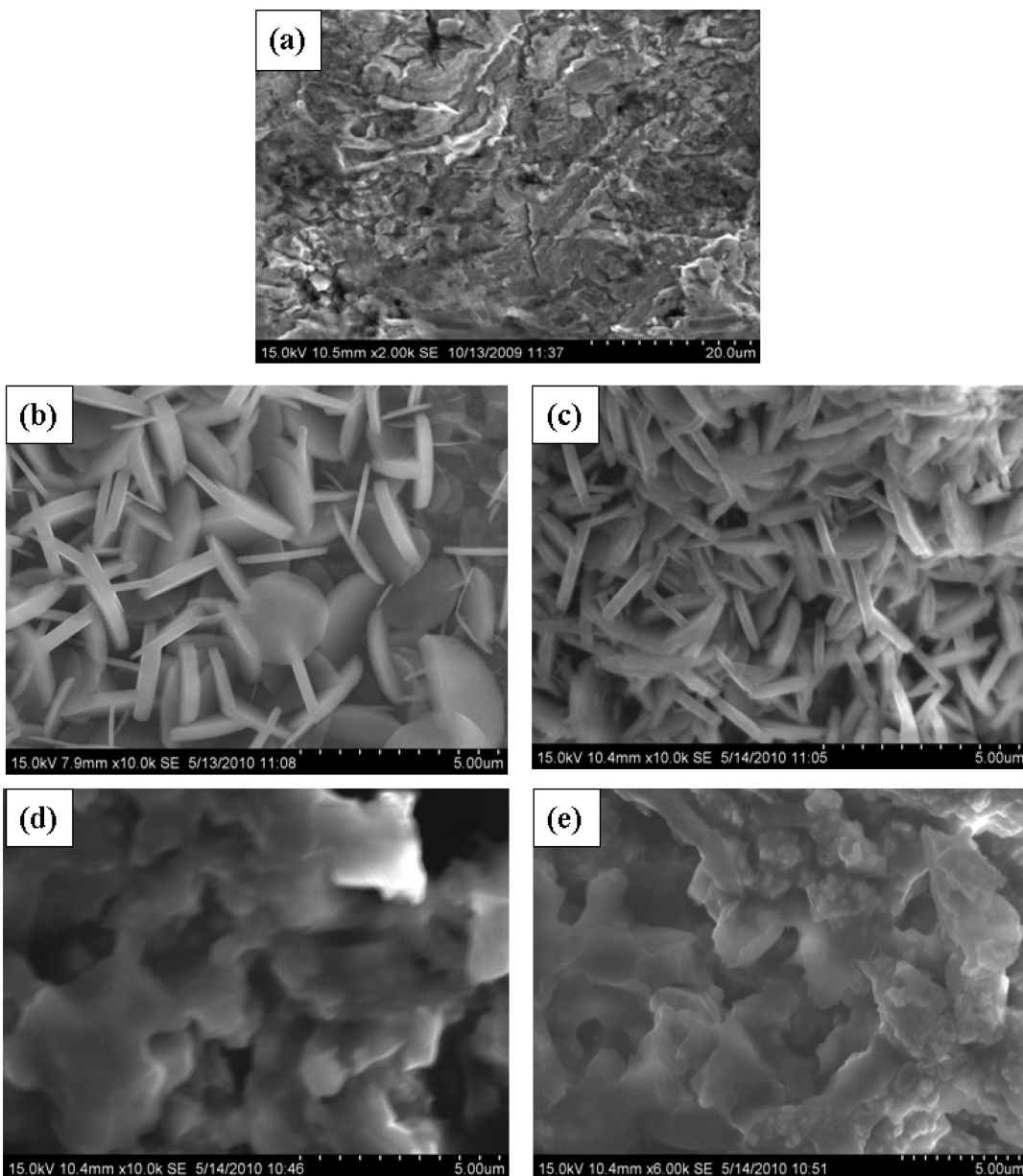


Figure 10. SEM images of brass: (a) blank and (b–e) inhibited complex formation of AMOPTD, AMPTD, APTD, and ANPTD.

group of AMOPTD are observed between 2963 and 3093 cm^{-1} , and the peak for the corresponding surface film is at 2925–2963 cm^{-1} . The strong band at 1642 cm^{-1} is due to the presence of N=O group. The symmetrical and asymmetrical C–NO₂ stretching vibrations of ANPTD are observed at 1342 and 1510 cm^{-1} , respectively, and the corresponding peaks for surface films of ANPTD are shifted to higher frequencies of 1347 and 1522 cm^{-1} , respectively.

3.8. SEM and EDS Analysis. The scanning electron photographs of the brass sample in the absence and presence of optimum concentrations of the studied thiadiazole derivatives are shown in Figure 10. The inhibited metal surface is smoother than the uninhibited surface, indicating the presence of a protective layer of adsorbed inhibitor preventing chloride attack in natural seawater. The micrographs of the brass surface after polarization experiment are analyzed. The brass surface in the absence of inhibitors appears to be covered with a layer of

corrosion products and is shown in Figure 10a. This is due to the attack of brass surface with aggressive chloride ions in natural seawater. The metallic surface seems to be not affected by corrosion in the presence of 10⁻³ M AMOPTD, AMPTD, APTD, and ANPTD (10⁻⁴ M) inhibitor molecules. This is due to the formation of copper and zinc complexes of studied thiadiazole derivatives that protect the brass surface against corrosion. The formation of complex with inhibitor is visible in the presence of AMOPTD, AMPTD, APTD, and ANPTD, and the micrographs are shown in Figure 10b–e. At the optimum concentration of the inhibitors, the surface is covered by a thin layer of inhibitor which effectively controls the dissolution of brass. The formation of the complex with inhibitors on the brass surface has higher stability and low permeability in aggressive solution than the uninhibited brass surface. Therefore, they show much better film properties, which seem to provide some corrosion protection to the metal beneath them by restricting

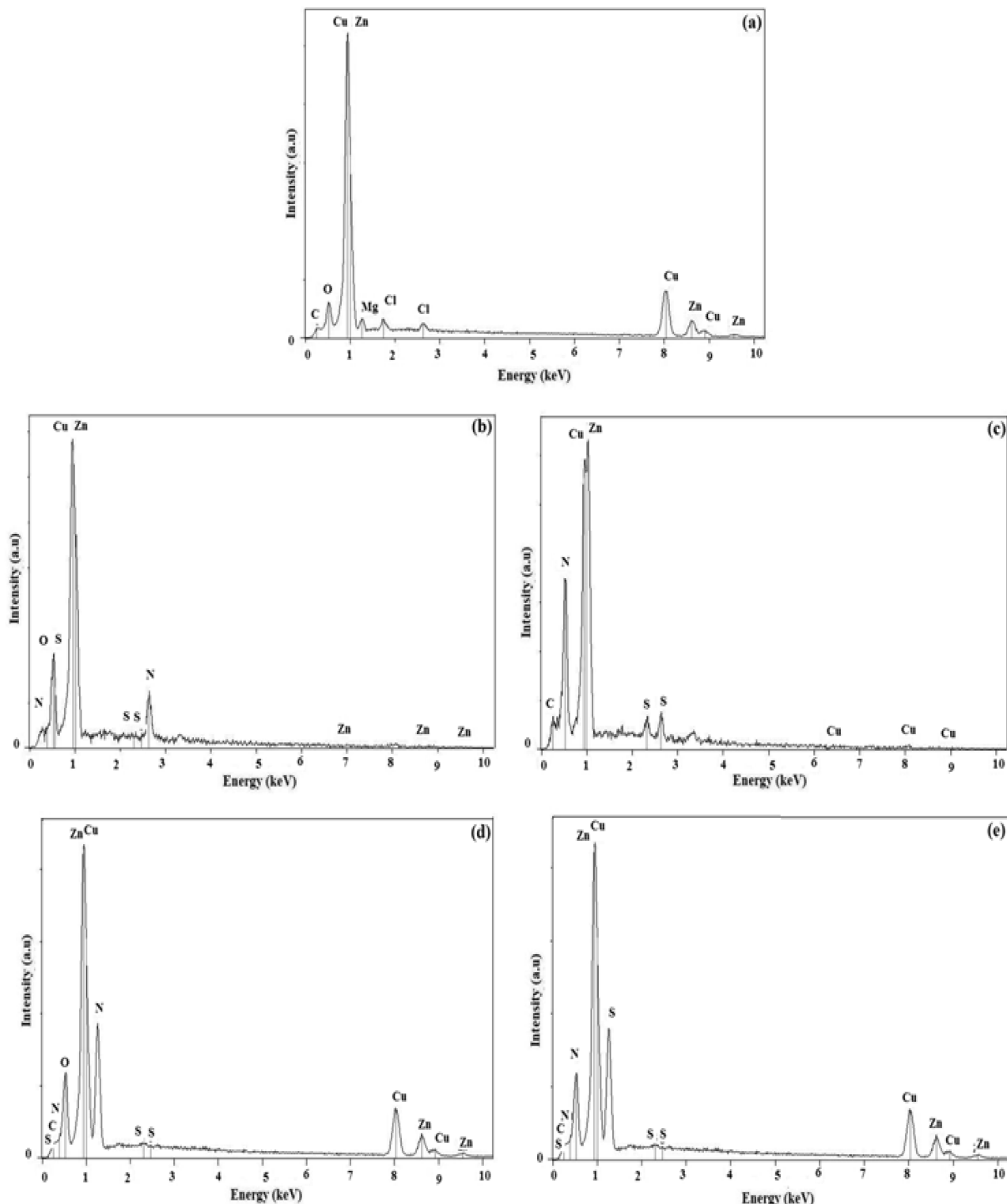


Figure 11. EDS profiles for brass surface: (a) blank, (b) AMOPTD, (c) AMPTD, (d) APTD, and (e) ANPTD.

the mass transfer of reactants and products between the bulk solution and the metal surface.

EDS spectra were used to determine the elements present on the brass surface before and after exposure to the inhibitor solution. It is also important to notice the existence of the nitrogen and sulfur atoms in the EDS spectra of the brass surface

corresponding to the sample immersed for 1 h in solution containing the optimum concentrations of AMOPTD, AMPTD, APTD, and ANPTD. Figure 11 presents the EDS spectra for the samples in the absence and presence of optimal concentrations of studied thiadiazole derivatives. In the absence of inhibitor molecules, the EDS spectra confirm the existence of chlorine

and oxygen along with copper and zinc due to the formation of Cu_2O and CuCl_2^- complex, which shows the passive film contained only by Cu_2O and CuCl_2^- . However, in the presence of the optimum concentrations of the AMOPTD, AMPTD, APTD, and ANPTD inhibitors, nitrogen and sulfur atoms are found to be present and coordinated with the brass surface, thus forming the complexes of the studied inhibitors on the brass surface. This indicates that the studied inhibitor molecules are adsorbed on the brass surface, thus protecting the brass surface against corrosion.

3.9. Mechanism of Corrosion Inhibition. The inhibition efficiency of an organic compound depends on many factors including the electronic structure, number of adsorption centers, mode of interactions with metal surface, molecular size, and chemical properties of the inhibitor being adsorbed. The inhibitor molecules can be adsorbed onto the metal surface through electron transfer from the adsorbed species to the vacant d orbital in the metal to form a coordinate type link.³³ It is well-known that the metal has coordination affinity toward nitrogen-, sulfur-, and oxygen-bearing ligands.

The studied compounds contain two iminic groups ($-\text{C}=\text{N}-$), one primary amino group, and one thio group of the thiadiazole ring besides the methoxyphenyl group in AMOPTD, the methyl-phenyl group in AMPTD, the pyridinyl group in APTD, and the nitrophenyl group in ANPTD, respectively. The unshared electron pairs on N and S are capable of forming a coordination bond with copper, enhancing the adsorption of the compounds on the metal surface. It is apparent that the adsorption of these thiadiazole derivatives on the brass surface could occur directly on the basis of donor behavior of the heteroatoms bearing the lone pair of electrons and the extensively delocalized π -electrons of the thiadiazole derivative molecules with the acceptor behavior of the vacant d orbitals of brass surface atoms.³⁴ AMOPTD was found to give excellent inhibition due to the presence of an additional electron-donating group ($-\text{OCH}_3$) on the thiadiazole derivative which increases the electron density. This leads to the strong electrostatic attraction of AMOPTD on the metal surface, thereby resulting in high inhibition efficiency. However, the poor performance of the compound ANPTD may be attributed to the presence of an NO_2 group in it. The nitro group is a strong electron-withdrawing group, and thus it reduces the π -electron density of the aromatic ring and the availability of π -electrons for interaction with copper is decreased. The poor inhibitive properties at low temperature besides the acceleration of corrosion at high temperature are also due to its specific electronic structure and the high dipole moment of ANPTD.

4. CONCLUSIONS

The corrosion behavior of brass was investigated by electrochemical measurements in natural seawater in the absence and presence of various concentrations of AMOPTD, AMPTD, APTD, and ANPTD at different temperatures. Analysis of the experimental data suggest that compounds AMOPTD, AMPTD, and APTD show good inhibiting properties that increase with inhibitor concentration, but ANPTD accelerates the corrosion process with increasing concentration due to the presence of an electron-withdrawing nitro group. EIS measurements indicate that the inhibitors examined hinder the corrosion process due to the increase of charge transfer resistance, film resistance, and Faradaic resistance related to the stabilization of corrosion products. The adsorption of the investigated inhibitor compounds was found to obey Langmuir's adsorption isotherm, indicating that the inhibition

process occurs via adsorption. The negative value of ΔG_{ads} obtained from this study indicates that these compounds are strongly spontaneously adsorbed on the brass surface. The values of the free energy of the adsorption reveal chemical adsorption. Thermodynamic adsorption parameters show that the studied inhibitors are adsorbed on the brass surface by an exothermic, spontaneous process.

Surface morphological studies such as FT-IR, SEM, and EDS analysis showed that a film of inhibitor is formed on the brass surface. The film inhibits the growth of oxides of copper and zinc and chlorides of copper and zinc. ICP-AES analysis reveals that the investigated inhibitors effectively control the dezincification of brass. The inhibition efficiency in natural seawater increases according to the order AMOPTD > AMPTD > APTD ≫ ANPTD.

■ AUTHOR INFORMATION

Corresponding Author

*Tel.: +91-44-22358659. Fax: +91-44-22200660. E-mail: nrajendran@annauniv.edu.

■ ACKNOWLEDGMENT

The author is greatly acknowledged to All India Council for Technical Education, New Delhi, India for the financial support under Research Promotion Scheme (RPS-167/2009-10).

■ REFERENCES

- (1) Jones, D. A. *Principles and Prevention of Corrosion*, 2nd ed.; Prentice-Hall: Upper Saddle River, NJ, 1996.
- (2) Poling, G. W. Reflection infra-red studies of films formed by benzotriazole on Cu. *Corros. Sci.* **1970**, *10*, 359.
- (3) Mansfeld, F.; Smith, T.; Parry, E. P. BTA as a Corrosion Inhibitor for Copper. *Corrosion* **1971**, *27*, 289.
- (4) Sinyavskii, V. S.; Kalinin, V. D. Marine Corrosion and Protection of Aluminum Alloys According to Their Composition and Structure. *Prot. Met.* **2005**, *41*, 347.
- (5) Emregul, K. C.; Atakol Corrosion inhibition of mild steel with Schiff base compounds in 1 M HCl. *Mater. Chem. Phys.* **2003**, *82*, 188.
- (6) Raicheva, S. N.; Aleksiev, B. V.; Sokolova, E. I. The effect of the chemical structure of some nitrogen- and sulphur-containing organic compounds on their corrosion inhibiting action. *Corros. Sci.* **1993**, *34*, 343.
- (7) Cheng, X. L.; Ma, H. Y.; Chen, S.; Yu, R.; Chen, X.; Yao, Z. M. Corrosion of stainless steels in acid solutions with organic sulfur-containing compounds. *Corros. Sci.* **1993**, *41*, 321.
- (8) Abd El Rehim, S. S.; Ibrahim, M. A. M.; Khaled, K. F. 4-Aminoantipyrine as an inhibitor of mild steel corrosion in HCl solution. *J. Appl. Electrochem.* **1999**, *29*, 593.
- (9) Sherif, E. S. M. Effects of 2-amino-5-(ethylthio)-1,3,4-thiadiazole on copper corrosion as a corrosion inhibitor in 3% NaCl solutions. *Appl. Surf. Sci.* **2006**, *252*, 8615.
- (10) Sherif, E. S. M.; Park, S. M. 2-Amino-5-ethyl-1,3,4-thiadiazole as a corrosion inhibitor for copper in 3.0% NaCl solutions. *Corros. Sci.* **2006**, *48*, 4065.
- (11) Blajiev, O.; Hubin, A. Inhibition of copper corrosion in chloride solutions by amino-mercapto-thiadiazol and methyl-mercapto-thiadiazol: an impedance spectroscopy and a quantum-chemical investigation. *Electrochim. Acta* **2004**, *49*, 2761.
- (12) Ravichandran, R.; Rajendran, N. Influence of benzotriazole derivatives on the dezincification of 65-35 brass in sodium chloride. *Appl. Surf. Sci.* **2005**, *239*, 182.
- (13) Ravichandran, R.; Nanjundan, S.; Rajendran, N. Corrosion inhibition of brass by benzotriazole derivatives in NaCl solution. *Anti-Corros. Methods Mater.* **2005**, *52*, 226.

- (14) Kabasakaloglu, M.; Kayak, T.; Sendil, O.; Asan, A. Electrochemical behaviour of brass in 0.1 M NaCl. *Appl. Surf. Sci.* **2002**, *193*, 167.
- (15) Ravichandran, R.; Nanjundan, S.; Rajendran, N. Effect of benzotriazole derivatives on the corrosion and dezincification of brass in neutral chloride solution. *J. Appl. Electrochem.* **2004**, *34*, 1171.
- (16) Badawy, W. A.; El-Egamy, S. S.; El-Azap, A. S. The electrochemical behaviour of leaded brass in neutral Cl^- and SO_4^{2-} media. *Corros. Sci.* **1995**, *37*, 1969.
- (17) Kim, B. S.; Piao, T.; Holer, S. N.; Park, S. M. In situ spectroelectrochemical studies on the oxidation mechanism of brass. *Corros. Sci.* **1995**, *37*, 557.
- (18) Ravichandran, R.; Nanjundan, S.; Rajendran, N. Effect of benzotriazole derivatives on the corrosion of brass in NaCl solutions. *Appl. Surf. Sci.* **2004**, *236*, 241.
- (19) Muralidharan, S.; Phani, K. L. N.; Pitchumani, S.; Ravichandran, S.; Iyer, S. V. K. Polyamino benzoquinone polymers—a new class of corrosion inhibitors for mild steel. *J. Electrochem. Soc.* **1995**, *142*, 1478.
- (20) Bereket, G.; Pinarbası, A. Electrochemical thermodynamic and kinetic studies of the behaviour of aluminium in hydrochloric acid containing various benzotriazole derivatives. *Corros. Eng., Sci. Technol.* **2004**, *39*, 308.
- (21) Santos, C. I. S.; Mendonca, M. H.; Fonseca, I. T. E. Corrosion of brass in natural and artificial seawater. *J. Appl. Electrochem.* **2006**, *36*, 1353.
- (22) Galicia, P.; Batina, N.; González, I. The Relationship between the Surface Composition and Electrical Properties of Corrosion Films Formed on Carbon Steel in Alkaline Sour Medium: An XPS and EIS Study. *J. Phys. Chem. B* **2006**, *110*, 14398.
- (23) McCafferty, E.; Hackerman, N. Double layer capacitance of iron and corrosion inhibition with polymethylene diamines. *J. Electrochem. Soc.* **1972**, *119*, 146.
- (24) Loveday, D.; Peterson, P.; Rodgers, B. Evaluation of Organic Coatings with Electrochemical Impedance Spectroscopy. *JCT CoatingsTech* **2004**, *1*, 88.
- (25) Lebrini, M.; Bentiss, F.; Vezin, H.; Lagrenée, M. The inhibition of mild steel corrosion in acidic solutions by 2,5-bis(4-pyridyl)-1,3,4-thiadiazole: Structure—activity correlation. *Corros. Sci.* **2006**, *48*, 1279.
- (26) Bentiss, F.; Lebrini, M.; Lagrenée, M. Thermodynamic characterization of metal dissolution and inhibitor adsorption processes in mild steel/2,5-bis(*n*-thienyl)-1,3,4-thiadiazoles/hydrochloric acid system. *Corros. Sci.* **2005**, *47*, 2915.
- (27) Durnie, W.; Marco, R. D.; Jefferson, A.; Kinsella, B. Development of a Structure-Activity Relationship for Oil Field Corrosion Inhibitors. *J. Electrochem. Soc.* **1999**, *146*, 1751.
- (28) Martinez, S.; Stern, I. Thermodynamics characterization of metal dissolution and inhibitor adsorption processes in the low carbon steel/mimosa tannin/sulfuric acid system. *Appl. Surf. Sci.* **2002**, *199*, 83.
- (29) Mu, G.; Li, X.; Liu, G. Synergistic inhibition between tween 60 and NaCl on the corrosion of cold rolled steel in 0.5 M sulfuric acid. *Corros. Sci.* **2005**, *47*, 1932.
- (30) Tang, L.; Mu, G.; Liu, G. The effect of neutral red on the corrosion inhibition of cold rolled steel in 1.0 M hydrochloric acid. *Corros. Sci.* **2003**, *45*, 2251.
- (31) Ogretir, C.; Mihci, B.; Bereket, G. Quantum chemical studies of some pyridine derivatives as corrosion inhibitors. *J. Mol. Struct.* **1999**, *488*, 223.
- (32) Lukovits, I.; Kalman, E.; Zucchi, F. Corrosion Inhibitors—Correlation between Electronic Structure and Efficiency. *Corrosion* **2001**, *57*, 3.
- (33) Cicileo, G. P.; Rosales, B. M.; Varela, F. E.; Vilche, J. R. Comparative study of organic inhibitors of copper corrosion. *Corros. Sci.* **1999**, *41*, 1359.
- (34) Maresca, K. P.; Rose, D. J.; Zubieto, J. Synthesis and characterization of a binuclear rhenium nitropyrazole complex $[\text{Re}_2\text{O}_3\text{Cl}_2(\text{PPh}_3)_2 \cdot (\text{C}_3\text{H}_2\text{N}_3\text{O}_2)_2]$. *Inorg. Chim. Acta* **1997**, *260*, 83.

■ NOTE ADDED AFTER ASAP PUBLICATION

After this paper was published online December 20, 2011, a correction was made to the Acknowledgment. The revised version was published January 3, 2012.